Structure of aqueous ammonium calcium nitrate glass former studied by neutron diffraction

1999 J. Phys.: Condens. Matter 11 7035

(http://iopscience.iop.org/0953-8984/11/37/301)

J. Phys.: Condens. Matter **11** (1999) 7035–7049. Printed in the UK PII: S0953-8984(99)97039-X

Structure of aqueous ammonium calcium nitrate glass former studied by neutron diffraction

S Ansell and G W Neilson

H H Wills Physics Building, University of Bristol, Tyndall Avenue, Bristol BS8 1TL, UK

Received 27 August 1998

Abstract. A neutron diffraction experiment was carried out on the glass-forming aqueous system of ammonium calcium nitrate tetrahydrate, ACN ($NH_4NO_3{\cdot}Ca(NO_3)_2{\cdot}4H_2O$). The method of isotopic substitution was used to determine the local structure round the NO_3^- ion, the hydrogen–hydrogen ($g_{HH}(r)$), the hydrogen–oxygen ($g_{OH}(r)$), and the nitrogen–hydrogen ($g_{N_2H}(r)$) radial pair distribution functions, in both the glassy (153 K) and liquid (303 K) states. The results show that significant changes occur on glassification. In particular, the nitrate ion exhibits an increase in the number of close hydrogen contacts and enhancement of its local structure. A microstructural model is proposed to explain the strong glass-forming ability of ACN.

1. Introduction

Ammonium nitrate and its compounds comprise a group of materials which exhibit a rich phase behaviour and are used for a variety of purposes by the chemical industry [1, 2]. Most importantly for the work described here, ammonium calcium nitrate tetrahydrate or ACN ($NH_4NO_3{\cdot}Ca(NO_3)_2{\cdot}4H_2O$) is an ideal candidate subject for a study of the structural aspects of glassification in a fragile glass. Although solid at room temperature, it is a stable liquid solution at 60 °C and forms a glass at the transition temperature (T_g), 203 K, upon cooling faster than a minimum quench rate of less than 1 K per hour! If the cooling rate is too slow in the supercooled region, it phase separates into ammonium nitrate and calcium nitrate tetrahydrate. Highly concentrated solutions of this kind are often referred to as hydrate melts, because there is insufficient water to complete the first hydration shells of all the constituent ions. Therefore short-range Coulombic interactions are assumed to exist between the ions. ACN is a mixture of strongly hydrophilic and weakly hydrophilic ions sharing a very small number of water molecules. The divalent calcium ion is the most hydrophilic of the three ions, Ca^{2+}, NH_4^+, and NO_3^-. In dilute solution, Ca^{2+} has a hydration number significantly greater than 6 with the water molecules in the first hydration sphere in fast exchange, $<10^{-10}$ s [3]. In various crystals Ca^{2+} has been found to have nine oxygen atoms within the first coordination sphere; examples include calcium nitrate tetrahydrate ($Ca(NO_3)_2{\cdot}4H_2O$) [4] and calcium nitrate dihydrate ($Ca(NO_3)_2{\cdot}2H_2O$) [5]. In hyperquenched glasses of dilute calcium nitrate solution, results from Raman spectroscopy have shown that the number of ion–ion contacts between the calcium and nitrate ions is larger than that in the liquid. By contrast, ACN hydrate melt will be complicated by the presence of the ammonium ion. However, because this ion has a lower charge density than Ca^{2+}, it might be anticipated that the Ca^{2+} will coordinate more strongly with the nitrate ion and prevent any phase separation caused by direct and extended NH_4^+–NO_3^- interactions.

0953-8984/99/377035+15$30.00

It is within this context that we have carried out a neutron diffraction isotopic substitution (NDIS) study of the changes that take place when ACN is glassified, and attempted to identify an appropriate structural signature associated with the glassification process. It will be recalled that, in the classic work of Angell and Sare, a correlation was established between the value of T_g and the anionic species in fragile glasses [6]. In their pioneering work on lithium chloride hydrated glasses, Dupuy, Jal and co-workers [7,8] showed that Cl^- hydration is indeed sensitive to glassification, a result recently confirmed by Ansell *et al* [9]. An important aspect of the present study is, therefore, to identify any changes in NO_3^- coordination on glassification of ACN.

Recall that the nitrate ion is planar, the oxygen atoms are negatively charged, and the central nitrogen atom is slightly positive with respect to a neutral atom [10]. The nitrate ion has been shown to have a water coordination which is strongly dependent on the counter-ion [11]; there are a diversity of possible hydration structures for the nitrate ion and it is thought that glassification will enable these to be more clearly identified. In addition, the current understanding of glassification is that the structure is determined by locally constrained rearrangements of the ions [12]. This would result in the hydration of the nitrate ion adopting its lowest energy state, which can be achieved with only those ions and molecules in the proximity of the nitrate ion at the glassification point. One potential problem in the study of the structure around nitrate ions is that the radial distribution functions calculated from neutron diffraction data are difficult to analyse because the nitrate ion is planar. This difficulty is more pronounced in crystals, glasses, and highly concentrated liquids where dynamical effects do not produce a spherical structure; the absence of a spherically symmetric electric field causes the first hydration shell to depend strongly on orientation. To help resolve this inherent difficulty in the data interpretation, the nitrogen–hydrogen pair correlation was also measured.

It has also been shown by neutron diffraction studies of simple aqueous fragile glass formers that the water structure is changed by the process of glass formation [8]. Moreover, the normal water hydration structure is strongly perturbed in highly concentrated electrolytic solutions [13]. Additionally water has a temperature-dependent dielectric constant which influences the number of ion–ion pairs in a solution. When the temperature is decreased, the dielectric constant increases [14] and the strength of the hydrogen bond formed between a hydrogen atom and an oxygen atom from two different water molecules increases also. If the water molecules are sufficiently mobile during the quenching process, it is expected that an increase in the number of hydrogen bonds will exist, giving rise to the formation of a hydrogen bond network. Consequently, the water structure was also investigated to determine how the glass-forming process affected that hydrogen bond network.

2. Experimental procedure and data analysis

Neutron diffraction experiments were carried out on the following six isotopically enriched samples:

(I) $Ca(^{Nat}NO_3)_2 \cdot {}^{Nat}ND_4\,{}^{Nat}NO_3 \cdot 4D_2O$,

(II) $Ca(^{15}NO_3)_2 \cdot {}^{Nat}ND_4\,{}^{15}NO_3 \cdot 4D_2O$,

(III) $Ca(^{Nat}NO_3)_2 \cdot {}^{Nat}NH_4\,{}^{Nat}NO_3 \cdot 4H_2O$,

(IV) $Ca(^{15}NO_3)_2 \cdot {}^{Nat}NH_4\,{}^{15}NO_3 \cdot 4H_2O$,

(V) $Ca(^{Nat}NO_3)_2 \cdot {}^{Nat}NH_4\,{}^{Nat}NO_3 \cdot 4H_2O$ (63% deuterium),

(VI) $Ca(^{Nat}NO_3)_2 \cdot {}^{Nat}NH_4\,{}^{Nat}NO_3 \cdot 4H_2O$ (35% deuterium).

The exact elemental fractions in each sample are listed in table 1 along with the mean scattering lengths from the sample elements in table 2. Samples containing $^{Nat}NO_3$ were made from 'Analar'-grade anhydrous $Ca(NO_3)_2$ which, prior to use, was heated to 300 °C in a vacuum chamber and then combined with the required amount of NH_4NO_3. This was dissolved in excess water with the correct deuterium content, and evaporated to the experimental concentration, in a stream of dry nitrogen. Samples containing $^{15}NO_3$ were made from $ND_4\,{}^{15}NO_3$ supplied by M.S.D; $Ca(^{15}NO_3)_2$ was made with an ion-exchange method to produce HNO_3 from $ND^{15}NO_3$ and adding in excess the acid to 'Analar' $CaCO_3$. The resulting acidic solution was filtered and dried to form $Ca(^{15}NO_3)_2$.

Table 1. The compositions of the samples used in the correction procedures. The sample number density was 0.0950 atoms Å^{-3} in the liquid state and 0.096 atoms Å^{-3} in the glassy state.

Sample	$C_{^{15}N}$	$C_{^{14}N}$	C_D	C_H	C_O	C_{Ca}
F_D^{Nat}	0.001	0.132	0.398	0.002	0.433	0.033
F_D^{15}	0.096	0.037	0.398	0.002	0.433	0.033
F_H^{Nat}	0.001	0.132	0.000	0.400	0.433	0.033
F_H^{15}	0.096	0.037	0.000	0.400	0.433	0.033
$F_{35\%D}^{Nat}$	0.001	0.132	0.140	0.260	0.433	0.033
$F_{63\%D}^{Nat}$	0.001	0.132	0.252	0.148	0.433	0.033

Table 2. The mean coherent scattering lengths (fm) of the constituent atoms of each sample.

Sample	Hydrogen	Nitrogen	Oxygen	Calcium
$F_D^{Nat}(Q)$	6.622	9.360	5.805	4.90
$F_D^{15}(Q)$	6.622	7.26	5.805	4.90
$F_H^{Nat}(Q)$	−3.741	9.360	5.805	4.90
$F_H^{15}(Q)$	−3.741	7.26	5.805	4.90
$F_{63\%}^{Nat}(Q)$	2.82	9.360	5.805	4.90
$F_{35\%}^{Nat}(Q)$	0.10	9.360	5.805	4.90

The diffraction data were collected on the 7C2 diffractometer at Saclay which was operated with neutrons of wavelength 0.7 Å. The samples were held at 303 K (liquid) and 153 K (glass). All the experiments were carried out in an 'orange' cryostat. The data were corrected for absorption, and multiple and incoherent scattering effects, and put on an absolute scale of b sr^{-1}/nucleus by reference to a vanadium standard [15]. These procedures gave six total scattering cross sections $F(k)$, for each temperature (figures 1(a), 1(b)).

The following notation is used for labelling the nitrogen atoms in the ACN, $Ca(N_{(2)}O_3)_2{\cdot}N_{(1)}D_4N_{(2)}O_3{\cdot}4D_2O$ (figure 1(a)/figure 1(b)). The first-order difference between the $F(Q)$s for samples I and II is given by

$$\Delta_{N_2}^{Deut}(Q) = F_D^{Nat}(Q) - F_D^{15}(Q)$$
$$= A[S_{N_2O}(Q) - 1] + B[S_{N_2D}(Q) - 1] + C[S_{N_2Ca}(Q) - 1] + D[S_{N_2N_2}(Q) - 1] \quad (1)$$

where

$$A = 2c_{N_2}c_O b_O(b_{^{Nat}N_2} - b_{^{15}N_2}) \qquad B = 2c_{N_2}c_H b_D(b_{^{Nat}N_2} - b_{^{15}N_2})$$
$$C = 2c_{N_2}c_{Ca}b_{Ca}(b_{^{Nat}N_2} - b_{^{15}N_2}) \qquad D = c_{N_2}^2((b_{^{Nat}N_2})^2 - (b_{^{15}N_2})^2).$$

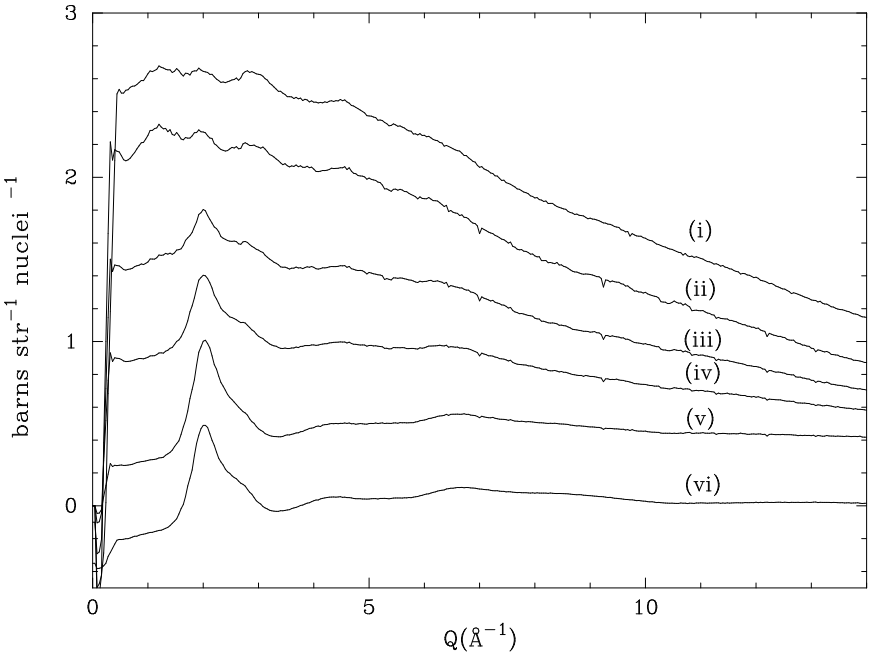

(a)

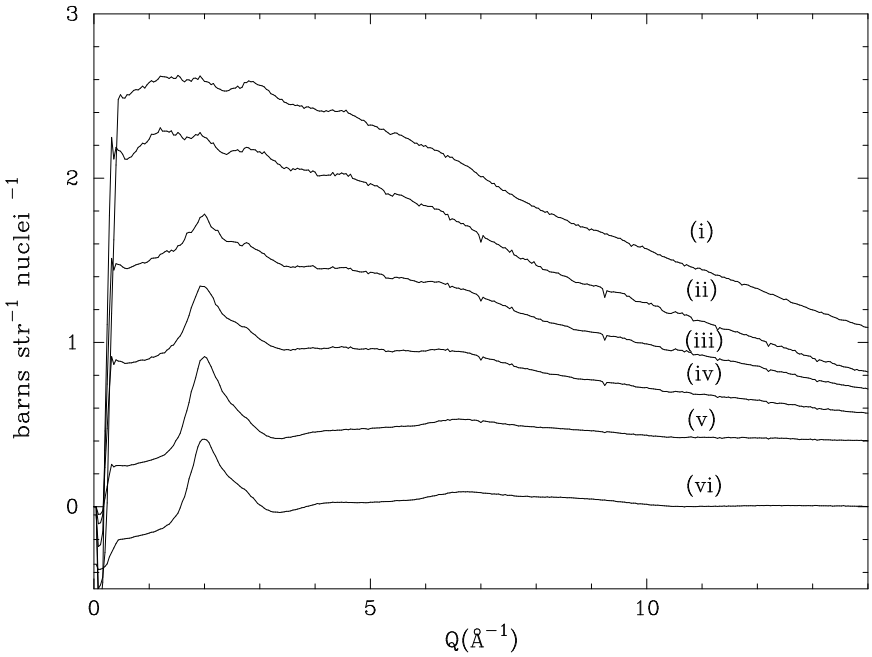

(b)

Figure 1. (a) The total structure factors for the six isotopically labelled mixtures of $NH_4NO_3{\cdot}Ca(NO_3)_2{\cdot}4H_2O$, (i) $F_H^{Nat}(Q)$ + 0.4, (ii) $F_H^{15}(Q)$, (iii) $F_{35\%}^{Nat}(Q)$, (iv) $F_{63\%}^{Nat}(Q)$, (v) $F_D^{Nat}(Q)$, (vi) $F_D^{15}(Q) - 0.4$, measured in the liquid state (303 K). (b) The total structure factors for the six isotopically labelled mixtures of $NH_4NO_3{\cdot}Ca(NO_3)_2{\cdot}4H_2O$, (i) $F_H^{Nat}(Q)$ + 0.4, (ii) $F_H^{15}(Q)$, (iii) $F_{35\%}^{Nat}(Q)$, (iv) $F_{63\%}^{Nat}(Q)$, (v) $F_D^{Nat}(Q)$, (vi) $F_D^{15}(Q) - 0.4$, measured in the glassy state (153 K).

c_α is the atomic concentration of the atom α whose neutron scattering length is b_α, and $S_{\alpha\beta}$ is the partial structure factor for the atom pair α–β. A similar expression for $\Delta_{N_2}^{Hydr}(Q)$ can be obtained from samples III and IV, where the 'D's representing deuterium atoms have been replaced with 'H's representing hydrogen atoms. The Fourier transformation of $\Delta_{N_2}(k)$ can be written as

$$G_{N_2}(r) = Ag_{N_2O} + Bg_{N_2H} + Cg_{N_2Ca} + Dg_{N_2N_2} + E \tag{2}$$

where

$$E = -(A + B + C + D).$$

The four first-order difference functions $\Delta_{N_2}(Q)$ (I–II and III–IV at -120 °C and 30 °C) and their corresponding Fourier transforms are displayed in figures 2 and 3 respectively. $G_{N_2}(r)$ is set to E for all r below the onset of the first intramolecular peak. The uncertainty in the inelasticity correction will exaggerate dips on either side of the relatively sharp intramolecular peak [16]. By the method of back-transformation it is possible to identify those features which are real and those which are artifacts. This has been taken into account when defining the accuracy of coordination numbers and interatomic distances. All the radial distribution functions given in this paper show the low-r portion of the Fourier transformation of the original $S(Q)$ without additional smoothing and with a window function which commences from 14 Å^{-1}. The low-r oscillation gives an indication of the accuracy of the structural information contained in the $g(r)$s. However, the oscillations themselves are a feature of the termination procedure and they decrease rapidly. Effects beyond the information limit of $r > 2\pi/Q_{Max}$ are not substantially affected by the smoothing procedures that we have used.

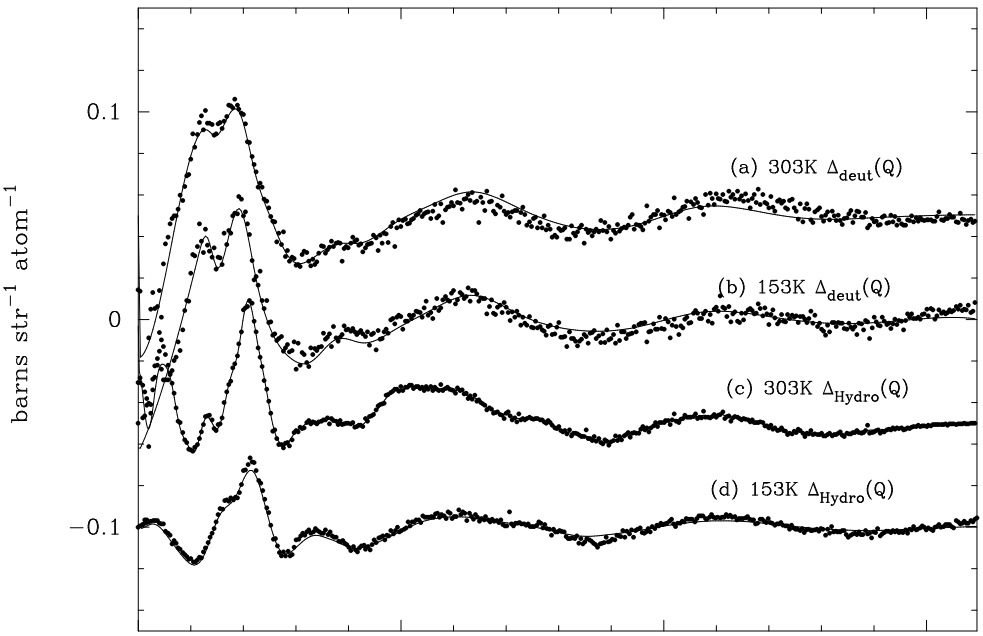

Figure 2. The first-order difference functions (a) $\Delta_{N_2}^{Deut}$ + 0.05 at 303 K, (b) $\Delta_{N_2}^{Deut}$ at 153 K, (c) $\Delta_{N_2}^{Hydr}$ − 0.05 at 303 K and (d) $\Delta_{N_2}^{Hydr}$ − 0.1 at 153 K. The solid lines represent the back-transforms of the respective $G_{N_2}(r)$s from figure 3.

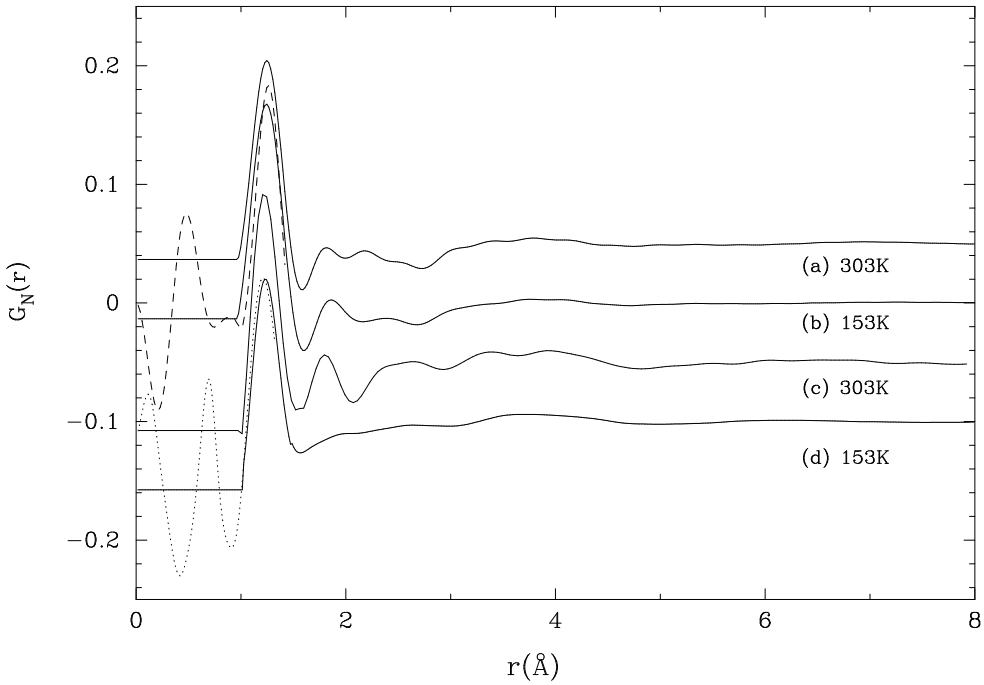

Figure 3. The real-space functions (a) $G_{N_2}^{Hydr}(r)$ + 0.05 at 303 K, (b) $G_{N_2}^{Hydr}(r)$ at 153 K, (c) $G_{N_2}^{Deut}(r) - 0.05$ at 303 K and (d) $G_{N_2}^{Deut}(r)$ at 153 K. Two functions, (b) and (d), are shown with minimum window functions applied to the $S(Q)$s (see the text).

The three pair distribution functions $g_{HH}(r)$, $g_{OH}(r)$, and $g_{N_2H}(r)$ were determined from the second-order difference method [17]. The calculation assumes that the hydrogen and deuterium occupy the ammonium and water sites with equal probability in the glass and the liquid. This assumption was validated by the observation that when water was evaporated under vacuum while the sample was maintained in the glassy state, the remaining material was found to have the same deuterium/hydrogen ratio as the initial glass.

Although $S_{HH}(Q)$ can, in principle, be determined from a combination of three $F(Q)$s, the results obtained were significantly noisier than those obtained when four $F(Q)$s were used. Consequently the latter combination of four $F(Q)$s was used to give

$$S_{HH}(Q) - 1 = \frac{[F_D^{Nat}(Q) - F_{35\%}^{Nat}(Q)] - [F_{63\%}^{Nat}(Q) - F_H^{Nat}(Q)]}{c_H^2(b_D - b_{35\%})(b_{63\%} - b_H)} \tag{3}$$

where b_D, $b_{63\%}$, $b_{35\%}$, b_H are the average scattering lengths for hydrogen in the total scattering cross sections $F_D^{Nat}(Q)$, $F_{63\%}^{Nat}(Q)$, $F_{35\%}^{Nat}(Q)$, and $F_H^{Nat}(Q)$ respectively. The values of the scattering lengths are given in table 2. The two resultant $S_{HH}(Q)$s, for the liquid and the glass, are shown in figure 4, and the Fourier transformation of $S_{HH}(Q) - 1$ enables the determination of the pair correlation functions $g_{HH}^{liq}(r)$ and $g_{HH}^{glass}(r)$ shown in figure 5.

It is not possible to determine uniquely the hydrogen–oxygen structure factor ($S_{OH}(Q)$) from the $F(Q)$ data sets. However, a good approximation is obtainable by using all six different total cross sections:

$$S'_{OH}(Q) = AF_H^{Nat}(Q) + BF_{35\%}^{Nat}(Q) + BF_{63\%}^{Nat}(Q) + DF_D^{Nat}(Q) + EF_H^{15}(Q) + FF_D^{15}(Q) \tag{4}$$

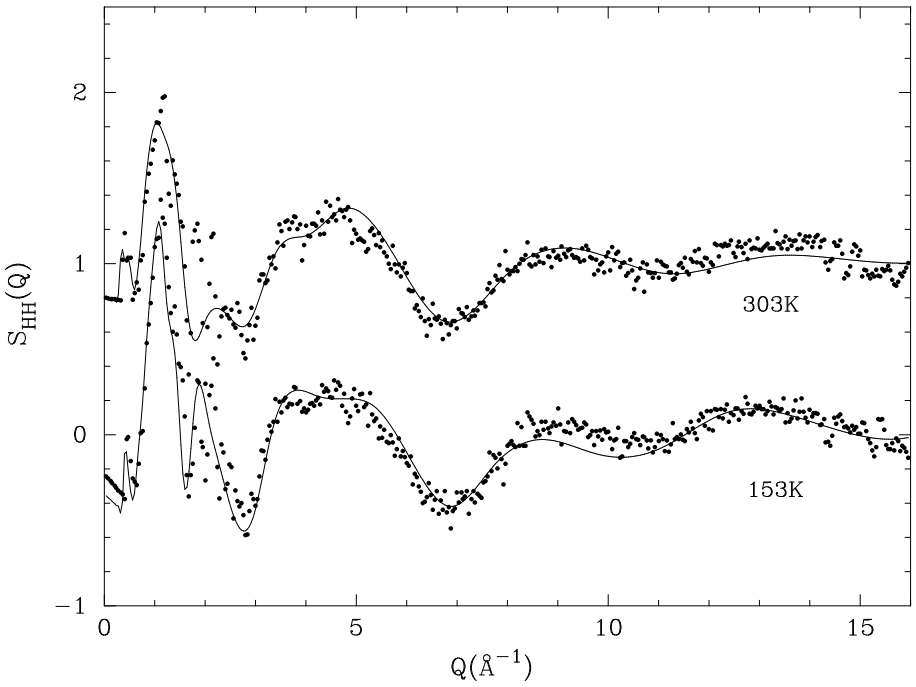

Figure 4. The second-order difference functions $S_{HH}(Q) - 1$ at 153 K and $S_{HH}(Q)$ at 303 K. The solid line represents the back-transforms of the respective $g_{HH}(r)$s from figure 5.

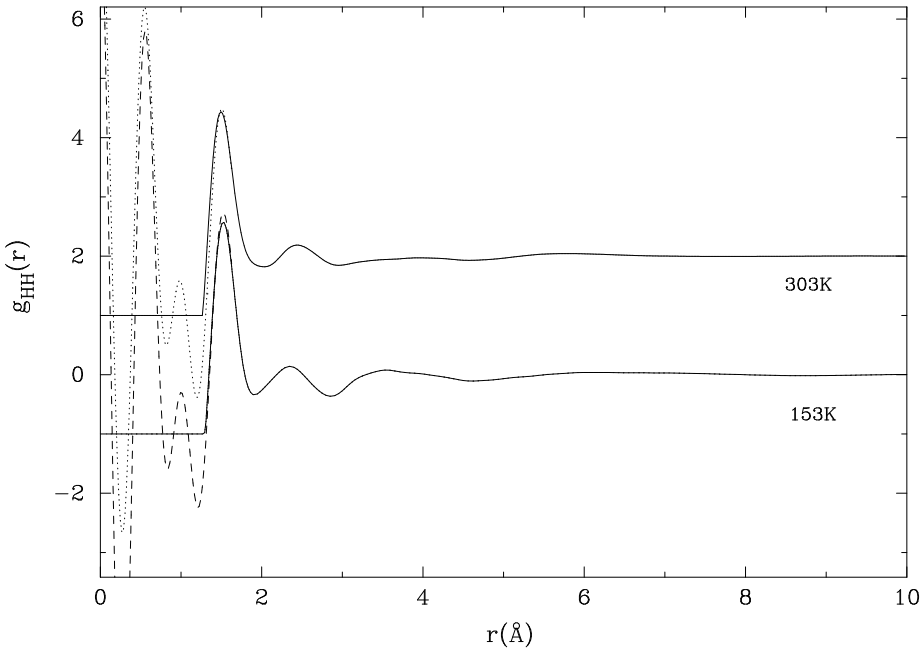

Figure 5. The radial pair distribution functions $g_{HH}(r)$ at 303 K and $g_{HH}(r) - 1$ at 153 K. Dotted lines are transforms with a minimum window function.

where $A, \ldots, F$ are given in table 3 (see also tables 4 and 5) and

$$S'_{OH}(Q) = S_{OH}(Q) + 0.065S_{CaH}(Q) + 0.123S_{NH}(Q). \tag{5}$$

Equation (5) shows that the $S'_{OH}(Q)$ term is dominated by $S'_{OH}(Q)$ (figure 6). Prior to Fourier transformation, the function $S'_{OH}(Q)$ was smoothed with a weighted cubic spline fit. This procedure removed noise-induced ripple from the $g'_{OH}(r)$s for liquid and glass (figure 7). The $g'_{OH}(r)$s also suffer from truncation problems which are similar to those which occur in the nitrate radial distribution function (figure 3) and the first peak of the pair distribution function of $g'_{OH}(r)$ is highly sensitive to the window function applied, giving rise to a variance in area of ≈30%, with a corresponding error in this particular coordination number.

Table 3. The weighting factors (mb sr^{-1}) of the different terms contributing to the nitrate first-order difference functions.

Difference	*A*	*B*	*C*	*D*	*E*
$\Delta_{N_2}^{Deut}(Q)$	18.80	19.80	0.92	7.93	−47.45
$\Delta_{N_2}^{Hydr}(Q)$	14.10	−8.39	0.92	6.21	−12.84

Table 4. The coefficients used in equation (4) to determine the $S'_{OH}(Q)$s.

Partial structure factor	*A*	*B*	*C*	*D*	*E*	*F*
$S'_{OH}(Q)$	13.61	5.74	5.85	−19.40	−21.35	21.35

Table 5. The structural parameters determined for the hydrogen–hydrogen radial pair distributions, $g_{HH}(r)$ (figure 5), for $NH_4NO_3{\cdot}Ca_2(NO_3)_2{\cdot}4H_2O$.

$g_{HH}(r)$	r_1	r_2	$\bar{n}^H_{H_1}$	$\bar{n}^H_{H_2}$
303 K	1.58 ± 0.03	2.85 ± 0.03	0.6 ± 0.3	5.0 ± 0.4
153 K	1.57 ± 0.03	2.85 ± 0.05	0.3 ± 0.3	5.0 ± 0.4

The points in the $g'_{OH}(r)$s below $r = 0.7$ Å were set equal to zero because no real structure can exist in this region. The results of back-transformations are shown in figure 6 and the difference between the back-transforms and the derived functions are slowly varying functions due to small additional inelastic effect, unaccounted for in the reduction procedures.

It was also possible to calculate $S_{N_2H}(Q)$ (and its Fourier transformation, $g_{N_2H}(r)$, from four of the $F(Q)$s ($F_D^{15}(Q)$, $F_D^{Nat}(Q)$, $F_H^{Nat}(Q)$ and $F_H^{15}(Q)$):

$$S_{N_2H}(Q) = \frac{[F_D^{Nat}(Q) - F_D^{15}(Q)] - [F_H^{Nat}(Q) - F_H^{15}(Q)]}{2c_{N_2}c_H(b_{^{Nat}N_2} - b_{^{15}N_2})(b_D - b_H)}. \tag{6}$$

The mean bound scattering lengths $b_{^{Nat}N}$, $b_{^{15}N}$, b_H, and b_D are shown in table 2. $S_{N_2H}(Q)$ was determined by a method similar to that used for $S_{OH}(Q)$, $S_{N_2H}(Q)$, and the back-transform is shown in figure 8 and the Fourier transform is shown in figure 9.

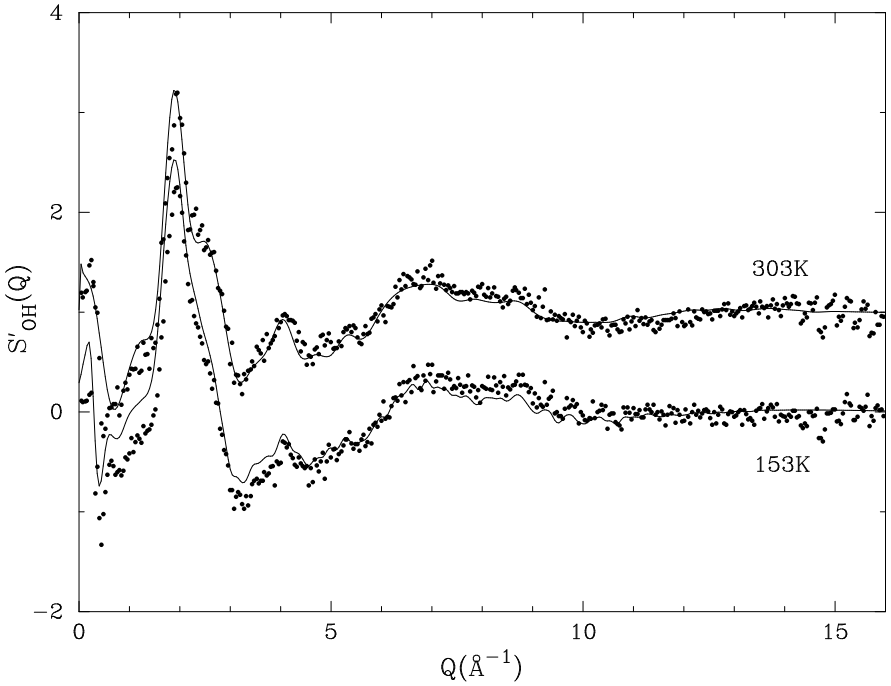

Figure 6. The second-order difference functions $S_{HO}(Q) - 1$ at 153 K and $S_{HO}(Q)$ at 303 K. The solid line represents the back-transforms of the respective $g_{HH}(r)$s from figure 7.

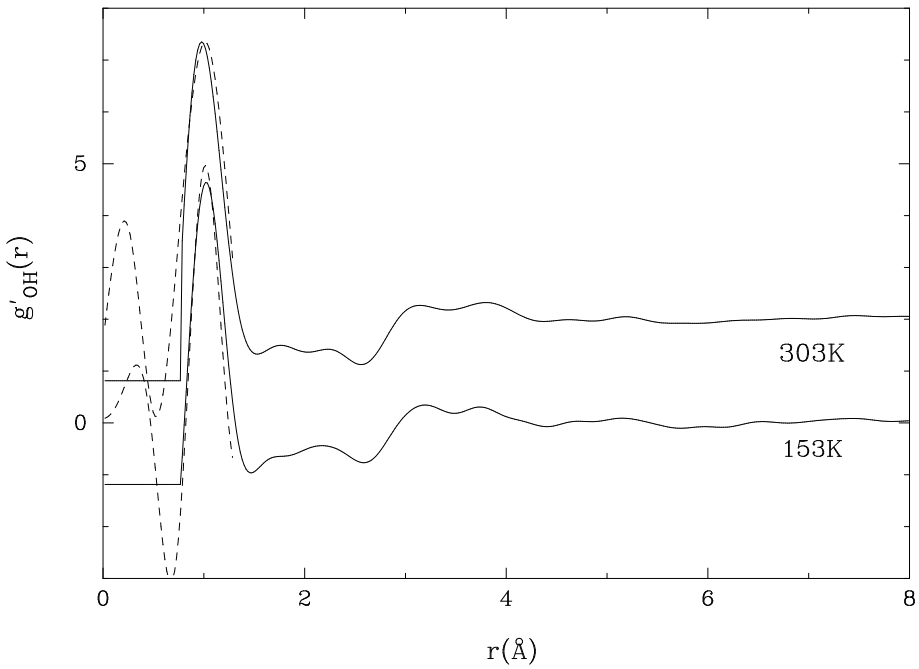

Figure 7. The radial pair distribution functions $g'_{HO}(r)$ at 303 K and $g'_{HO}(r) - 1$ at 153 K. (Note: the value of $g'_{HO}(0) - 1 = -1.187$.) Dotted lines are transforms with minimum window functions applied to the $S(Q)$s.

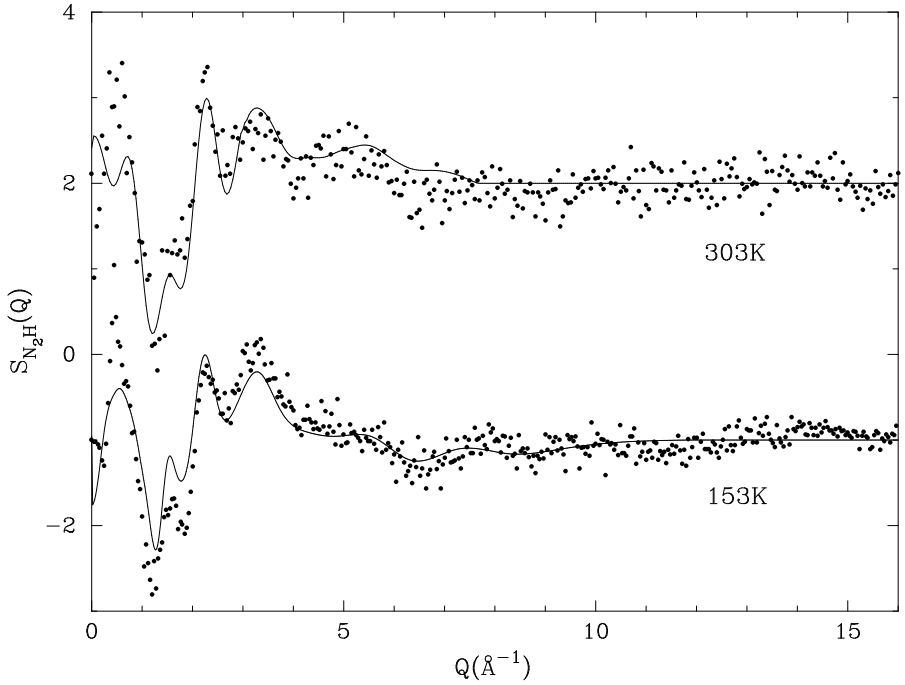

Figure 8. The second-order difference functions $S_{N_2H}(Q) - 1$ at 153 K and $S_{N_2H}(Q) + 1$ at 303 K. The solid line represents the back-transforms of the respective $g_{N_2H}(r)$s from figure 9.

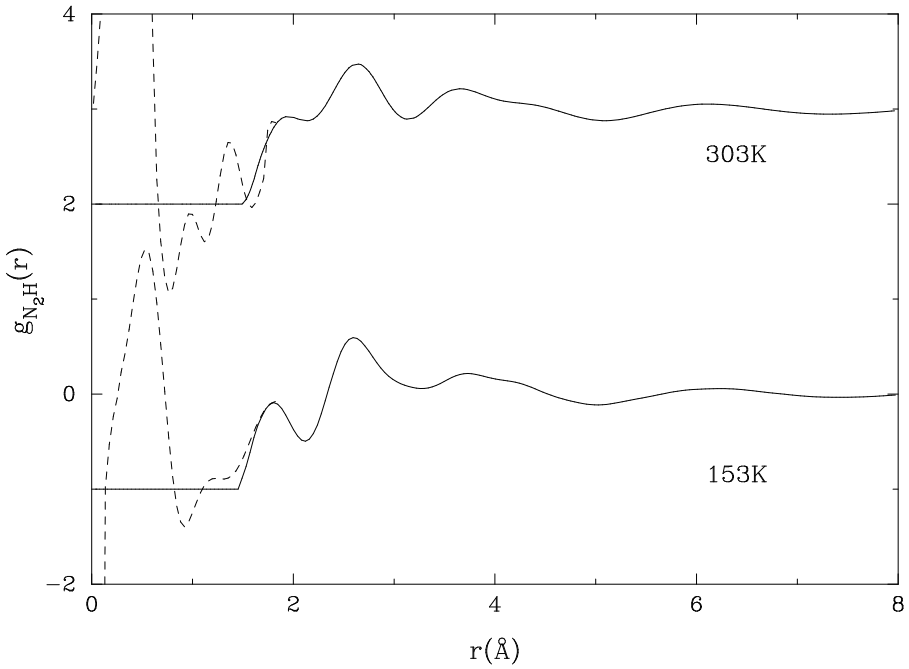

Figure 9. The radial pair distribution functions $g_{N_2H}(r)$ at 303 K and $g_{N_2H}(r) - 1$ at 153 K. Dotted lines are transforms with minimum window functions applied to the $S(Q)$s.

3. Discussion

3.1. The nitrate-ion coordination

The results for the liquid and glass are, as might be anticipated, in close agreement with each other, and similar to those found in previous work [16]. The strong first peak, which is at $r = 1.23 \pm 0.03$ Å in all four $G_{N_2}(r)$s, corresponds to the intramolecular N–O bond and is in excellent agreement with previous experimental determinations of this distance. Integration of this peak gave values between 2.9 and 3.1 which gives credence to the data analysis procedures employed.

Inspection of the liquid radial distribution functions shows that they are relatively featureless beyond the region of the intramolecular peak; the hydrogen-containing liquid ($G_{N_2}^{Hydr}(r;\ 303\ K)$) shows slightly more contrast due to the negative scattering length of the hydrogen atoms. Although this structure is the signature of a disordered nitrate-ion arrangement within the material, it is also consistent with ordering along the different symmetry axes of the planar nitrate ion. It is known from IR spectroscopy that in the liquid the nitrate ion is rotating; it is therefore unlikely that $G_{N_2}(r)$ will contain contributions which arise from this because of its non-radial aspect.

The $G_{N_2}^{Deut}(r)$ and $G_{N_2}^{Hydr}(r)$ functions obtained by Adya and Neilson [16] for $NH_4NO_3{\cdot}H_2O$ at 100 °C show very similar features, suggesting that the nitrate ion has very little influence on the structure within the liquid, and can be considered purely in terms of its space-filling property. The two glassy $G_{N_2}^{*}(r)$s show significantly stronger and better defined features than are observed for the liquid. There are three additional r-space features present in the deuterated glass $G_{N_2}^{glass}(r)$ beyond the intermolecular oxygen peak at 1.90 Å, 2.8 Å, and 3.8 Å. It was found that by applying different window functions the intramolecular peak itself can only be broadened. This feature in the hydrogenated $G_{N_2}^{Hydr}(r;\ 153\ K)$ is only just positive, indicating that it has a significant content of hydrogen atoms. A comparison of the 2.8 Å feature between the hydrogen and deuterium $G_{N_2}(r;\ 153\ K)$s shows that the feature is composed of several different atoms including hydrogen. The third larger feature at ≈3.8 Å is consistent with a loosely coordinated second shell.

3.2. Hydrogen–hydrogen pair correlation, $g_{HH}(r)$

The hydrogen–hydrogen radial pair distribution functions ($g_{HH}(r)$) for the liquid and the glass in figure 5 both show a lack of structure beyond 5 Å, which demonstrates that there is no hydrogen bond network spanning either the liquid or the glass. The water molecules and ammonium ions are not strongly coordinated to any one specific ion, and the calcium ion retains a four- (or more) site configuration. Otherwise, cross coordination of the hydrogen would result in visible structure at larger distances than is observed. The fourfold coordination might have been expected considering the calcium ion's known affinity for water, and also from the structure of the calcium nitrate tetrahydrate crystal which shows that the calcium ion is fourfold coordinated to the oxygen atoms of the water molecules [4].

The first and largest peak of $g_{HH}(r)$ arises from the intramolecular H–H coordination of the water and the ammonium ion. The peak is best fitted by two Gaussians centred at 1.58 ± 0.03 Å due to water molecules and 1.85 ± 0.03 Å due to the ammonium ions for the liquid and 1.57 ± 0.03 Å and 1.80 ± 0.03 Å for the glass. The H–H coordination number, $\bar{n}_H^H$, is calculated from the equation

$$\bar{n}_H^H = 4\pi\rho c_H \int_{r_1}^{r_2} g_{HH}(r) r^2\, dr \tag{7}$$

where r_1 and r_2 are the positions of the minima that span the peak in $g_{HH}(r)$. The two Gaussian peaks have identical $\bar{n}_H^H$s for the liquid and glass with a value of 1.4 ± 0.2 atoms for the first and 0.3 ± 0.2 atoms for the second peak. The total for $\bar{n}_H^H = 1.7 \pm 0.3$ is in good agreement with the expected value of 1.66 (this value represents the weighted average over concentration of the water hydrogen atoms and the ammonium hydrogen atoms with one and three intermolecular neighbours respectively). Thus the ammonium ion remains predominantly in the ionic form NH_4^+ at both temperatures.

The second smaller feature in the $g_{HH}(r)$s centred at 2.47 ± 0.03 Å for the liquid and 2.43 ± 0.03 Å for the glass can accommodate 2.2 ± 0.3 hydrogen atoms in both phases, and must be associated with two molecules containing hydrogen atoms. One possible explanation of the origin of this peak is that it could arise from two water molecules hydrogen bonded together. However, this is thought unlikely as the interaction with ions would be much stronger. The more probable explanation of the peak at ≈2.45 Å is that it arises from the formation of an NH_4^+–H_2O pair, in which the oxygen of the water molecule H bonds to two of the NH_4^+'s hydrogen atoms.

Although, this explanation accounts for some of the hydrogen in the 2.45 Å peak, it cannot explain the total contribution to this peak. To help explain the additional amount of hydrogen in this peak there must be at least some distant H_2O–H_2O or H_2O–NH_4^+ correlations via an intermediate-spacing ion, with Ca^{2+} the most likely candidate (see section 3.5).

3.3. Hydrogen–oxygen pair correlation, $g'_{OH}(r)$

The hydrogen–oxygen radial pair distribution functions ($g'_{OH}(r)$) for the liquid and glass are shown in figures 6 and 7. Recall that from equation (5) we obtain

$$g'_{OH}(r) = g_{OH}(r) + 0.065 g_{HCa}(r) + 0.123 g_{N_1H}(r). \tag{8}$$

As anticipated, both $g'_{OH}(r)$s are dominated by a peak at 0.98 ± 0.03 Å (liquid) and 0.99 ± 0.03 Å (glass). Integration over these peaks gives the values of $\bar{n}_H^O$ of 1.2 ± 0.3 hydrogen atoms for the liquid and 1.0 ± 0.3 hydrogen atoms for the glass. This peak is made up from the molecular contributions of O–H of the H_2O molecules and the N–H contribution of the NH_4^+ ions. The expected contributions are 0.5 atoms from the NH_4^+ and 0.6 atoms from the H_2O giving a total of 1.1 atoms which is consistent with both the liquid and glass experimental results. This gives us confidence both in the data reduction methods and that significant information has not been lost due to the limited Q-range in the $S'_{OH}(Q)$s.

The $g'_{OH}(r)$s also show peaks at 1.8 Å and 2.2 Å. We identify these as due only to H–O bonds, since we expect that because of their charge and size the NH_4^+ ions will have an insignificant number of hydrogen-bonded neighbours. The peak at 1.8 Å will have strong contributions from NH_4^+–NO_3^- contact pairs and the 2.2 Å peak expected to have a strong contribution from hydrogen-bonded H_2O–H_2O pairs. Comparison between the glass and liquid structures (table 6; see also table 7) shows that there is a slight increase in the coordination of the 2.2 Å peak from 0.6 ± 0.3 to 0.9 ± 0.3 upon glassification. This supports the hypothesis (section 3.5) of increasing Ca^{2+}–NO_3^- contacts within the glass that would lead to an increase in the number of hydrogen bonds within the glass.

The feature in at 3.3 Å cannot be directly interpreted because it is predominantly a combination of hydrogen atoms on both the NH_4^+ cation and water molecules together with the oxygen atoms of NO_3^- and H_2O. The presence of so many interacting units, and hence the large number of local environments, leads to a rapid smoothing of the features in $g'_{OH}(r)$ beyond 5 Å.

Table 6. The structural parameters determined for the hydrogen–oxygen radial pair distributions, $g'_{OH}(r)$ (figure 7), of $NH_4NO_3{\cdot}Ca(NO_3)_2{\cdot}4H_2O$.

$g'_{OH}(r)$	r_1	r_2	r_3	$\bar{n}^{O}_{H_1}$	$\bar{n}^{O}_{H_2}$	$\bar{n}^{O}_{H_3}$
303 K	0.98 ± 0.03	1.77 ± 0.08	2.2 ± 0.08	1.2 ± 0.3	0.3 ± 0.2	0.4 ± 0.2
153 K	0.99 ± 0.03	1.74 ± 0.08	2.2 ± 0.08	1.0 ± 0.3	0.2 ± 0.2	0.9 ± 0.3

Table 7. The structural parameters determined for the nitrogen–hydrogen radial pair distributions, $g_{N_2H}(r)$ (figure 9), of $NH_4NO_3{\cdot}Ca_2(NO_3)_2{\cdot}4H_2O$.

$g_{N_2H}(r)$	r_1	r_2	$\bar{n}^{N}_{H_1}$	$\bar{n}^{N}_{H_2}$
303 K	1.88 ± 0.03	2.85 ± 0.03	0.6 ± 0.3	5.0 ± 0.4
153 K	1.88 ± 0.03	2.85 ± 0.05	0.3 ± 0.3	5.0 ± 0.4

3.4. Nitrogen–hydrogen pair correlation, $g_{N_2H}(r)$

The nitrogen–hydrogen radial pair distribution functions ($g_{N_2H}(r)$) for the liquid and glass are shown in figure 9. The most striking observation is the peak at 1.88 Å which is much more pronounced in the glass. Integration under the peak using equation (7) shows that it contains 0.6 ± 0.3 atoms in the glass and 0.3 ± 0.2 atoms in the liquid. The position of this peak is strange because in stable nitrate crystals it is normal for the hydrogen to be close to the plane of NO_3^- [18] (figure 10) since the oxygen atoms on NO_3^- carry a fractional negative charge, whilst the central nitrogen atom has a fractional positive charge (the total sum of the charges is -1). This gives a N–H distance of $\approx$2.8 Å. Interestingly, however, in most of the simple proton-rich nitrate-containing crystals (e.g. $HNO_3{\cdot}3H_2O$ [20] and $NH_4{\cdot}HNO_3{\cdot}3H_2O$ [21]) the NO_3^- has two axial hydrogens at a distance of 1.75 Å. This indicates that although the site is available in normal aqueous solutions it is not often occupied; water molecules prefer to form hydrogen bond networks. By contrast, the evidence from the work presented above is that in a tightly packed geometry with an excess of hydrogen, the site must be occupied. Moreover,

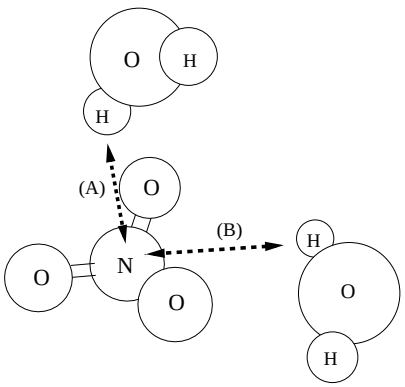

(A) Axial Separation, N-H distance = 1.75A

(B) Radial Separation, N-H distance = 2.05A

Figure 10. The axial and planar positions that a water molecule may adopt around a nitrate ion in solution.

the occupation of this site in the glassy state by hydrogen atoms suggests that on glassification either the ammonium or water are removed from another site and forced to take up this less preferred position.

It is therefore postulated that the hydrophilic Ca^{2+} localizes the oxygen atoms of both the H_2O and the NO_3^- on glassification. This process removes two of the three planar sites of NO_3^- available to the hydrogen of the water molecules or ammonium ions, and explains why so few sites are available in the glass.

3.5. Overview of results and conclusions

The results above provide an insight into the mechanism by which the atomic structure of ACN relates to its strong glass-forming tendency. It is helpful to examine a possible structural scenario of the ACN mixture and identify the appropriate signatures associated with glassification. When the mixture is liquid, the Ca^{2+} cannot distinguish between contacts with the oxygen of NO_3^- and the oxygen atoms of H_2O because the exchange rate of this hydration will be extremely fast ($<10^{-10}$ s). As the system cools, the nitrate oxygen will be preferred

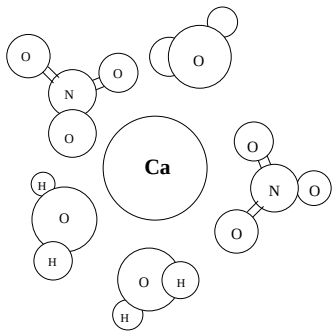

(a) Glass

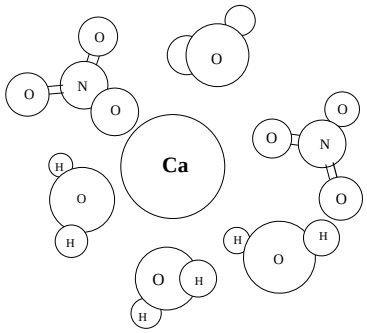

(b) Liquid

Figure 11. A proposed structure for the Ca^{2+} hydration in ACN in (a) glass and (b) liquid, showing the NO_3^- ions having one oxygen contact in the liquid and two oxygen contacts in the glass.

by the Ca^{2+} rather than the oxygen of the water molecules. The relatively high ion density means that ion pairs can form readily due to strong ion–ion bonding. In addition, the NO_3^- can contribute two oxygen atoms to the Ca^{2+}'s nearest-neighbour shell. Thus if a nitrate ion has one oxygen atom in contact with a Ca^{2+}, and a water molecule becomes disconnected from the Ca^{2+}, then the nitrate ion will adjust itself to fill the vacancy and stabilize glassification. By contrast, phase separation will occur if the nitrate ions detach themselves from the Ca^{2+}, leaving space for the water molecules to attach themselves to the Ca^{2+}. If phase separation does not occur at rapid cooling rates, the structure that the system is forced to adopt is one in which some of the water molecules have been screened out from the Ca^{2+}. The water molecules will not be completely randomly distributed but will find their most stable configuration without displacing the nitrate ions. With the NO_3^- motion becoming arrested in the glass, the hydrogen atoms of the water molecule and NH_4^+ will be able to adopt positions much closer to the NO_3^- ions than in the liquid, potentially exploring the asymmetry of the NO_3^- to adopt a polar position above or below the NO_3^- (figure 10). This type of structure is also seen in some crystals [19]. To summarize, the evidence for this model of NO_3^- bonding in its plane to Ca^{2+} and with water molecules at axial sites (figures 11(a), 11(b)) is further substantiated by structural information obtained for hydrogen-rich crystal, and from the increase in nitrogen–hydrogen coordination in the glass.

Acknowledgments

The authors are grateful to Dr J Cooper (ICI) for helpful contributions to the discussions, and to ICI and the EPSRC for a CASE award to S Ansell. We also thank Dr M C Bellissent-Funel for her help with the neutron diffraction experiments at Saclay.

References

[1] Oxley J C, Kaushik S M and Gilson N S 1992 *Thermochim. Acta* **212** 77
[2] Jarvis S C, Stockdale E A, Shepherd M A and Powlson D S 1996 *Adv. Agron.* **57** 187
[3] Friedman H L 1985 *Chim. Scr.* **25** 42
[4] Leclaire A and Monier J 1970 *C. R. Acad. Sci., Paris* C **271** 1555
[5] Morosin B 1970 *Acta Crystallogr.* B **26** 386
[6] Angell C A and Sare E J 1970 *J. Chem. Phys.* **52** 1058
[7] Jal J F, Soper A K, Carmona P and Dupuy J 1991 *J. Phys.: Condens. Matter* **3** 551
[8] Dupuy J, Jal J F and Cheiux P 1991 *J. Mol. Struct.* **250** 315
[9] Ansell S, Dupuy-Philon J, Jal J F and Neilson G W 1997 *Chem. Phys. Lett.* **278** 21
[10] Wyatt J F, Hillier I H, Saunders V R, Conner J A and Barber M 1971 *J. Chem. Phys.* **25** 395
[11] Neilson G W, Ansell S and Wilson J 1995 *Z. Naturf.* a **50** 247
[12] Zarzycki J 1991 *Glasses and the Vitreous State* (Cambridge: Cambridge University Press)
[13] Tromp R H, Neilson G W and Soper A K 1992 *J. Chem. Phys.* **11** 8466
[14] Irish D E and Jarv T 1983 *Appl. Spectrosc.* **37** 50
[15] Poncet P F J 1997 Subtraction and attenuation corrections for liquid samples confined within two coaxial cylinders *ILL Report* 77PO15S
[16] Adya A K and Neilson G W 1990 *Mol. Phys.* **69** 747
[17] Neilson G W and Enderby J E 1983 *Proc. R. Soc.* A **390** 353
[18] Neilson G W and Enderby J E 1982 *J. Phys. C: Solid State Phys.* **15** 2347
[19] Mildner D F R, Pelizzari C A and Carpenter J M 1977 *Acta Crystallogr.* A **33** 954
[20] Luzzati V 1953 *Acta Crystallogr.* **6** 152
[21] Mildner D F R and Carpenter J M 1977 *Acta Crystallogr.* A **33** 932